

Unprecedented Fluorophore Photostability Enabled by Low-Loss Organic Hyperbolic Materials

Yeon Ui Lee, Shilong Li, Steven Edward Bopp, Junxiang Zhao, Zhaoyu Nie, Clara Posner, Sui Yang, Xiang Zhang, Jin Zhang, and Zhaowei Liu*

The dynamics of photons in fluorescent molecules plays a key role in fluorescence imaging, optical sensing, organic photovoltaics, and displays. Photobleaching is an irreversible photodegradation process of fluorophores, representing a fundamental limitation in relevant optical applications. Chemical reagents are used to suppress the photobleaching rate but with exceptionally high specificity for each type of fluorophore. Here, using organic hyperbolic materials (OHMs), an optical platform to achieve unprecedented fluorophore photostability without any chemical specificity is demonstrated. A more than 500-fold lengthening of the photobleaching lifetime and a 230-fold increase in the total emitted photon counts are observed simultaneously. These exceptional improvements solely come from the low-loss hyperbolic dispersion of OHM films and the large resultant Purcell effect in the visible spectral range. The demonstrated OHM platform may open up a new paradigm in nanophotonics and organic plasmonics for super-resolution imaging and the engineering of light–matter interactions at the nanoscale.

Fluorescence microscopy^[1] has been employed extensively to unveil sophisticated properties of specimens that cannot be seen with traditional microscopes and has thereby become an indispensable tool in numerous important applications in medicine,^[1] environmental studies,^[2] food sanitation,^[3] biological research,^[4] and industry.^[5] However, these fluorescence-based sensing and imaging methods suffer from irreversible photobleaching^[6] of fluorophores (i.e., a loss of their ability

to fluoresce due to the photon-induced damage), which restricts the total number of emitted photons from each fluorophore. This photodegradation process eventually limits the maximum signal-to-noise ratio (SNR) and thus the sensitivity of a sensor^[2,5] or the resolution of an image.^[7,8] Therefore, it is crucial to enhance the fluorophore's photostability in order to improve the overall performance of fluorophore-based sensing and imaging systems.

Enormous efforts have been devoted to the enhancement of fluorophore photostability by varying either chemical or optical environments. The former method includes the introduction of chemical reagents.^[9] However, these chemical reagents have to be carefully selected in order to avoid unintentional reactions or interactions with the

specimens to be imaged. In another aspect, when the optical environment is modified, e.g., by using plasmonic nanostructures,^[10–13] the photobleaching of a fluorophore is suppressed due to an enhancement of its spontaneous emission process. This phenomenon is known as Purcell effect and is caused by the enhanced photonic local density of states (LDOS) near the corners of the plasmonic nanostructures. Nevertheless, the high spatial locality of LDOS contributed by the plasmonic nanostructures not only introduces an additional complexity associated with nanofabrication but also substantially limits their potential applications where the performance of any locations on an interested plane cannot be sacrificed, e.g., wide-field imaging and sensing.


In a different context, hyperbolic materials^[14,15] (i.e., the optical materials with a hyperbolic dispersion) have been the subject of extensive investigation over the past decade for their large potential in broad applications such as super-resolution imaging,^[16,17] refractive index sensing,^[18] engineering of optical nonlinearities,^[19] and enhancement of spontaneous emission.^[20,21] It has been demonstrated that hyperbolic polariton modes supported by the hyperbolic materials lead to a strong and broadband Purcell effect even in their planar form.^[22–26] Therefore, a layer of hyperbolic materials would be an ideal platform to improve the photostability of a fluorophore uniformly over the entire planar surface.^[27] However, the nonradiative nature of these hyperbolic polariton modes and the inevitable material loss contributed from the metallic components of traditional hyperbolic metamaterials (HMMs) present major

Dr. Y. U. Lee, Dr. S. Li, J. Zhao, Prof. Z. Liu
 Department of Electrical and Computer Engineering
 University of California, San Diego
 San Diego, 9500 Gilman Drive, La Jolla, CA 92093, USA
 E-mail: zhaowei@ucsd.edu

S. E. Bopp, Prof. Z. Liu
 Materials Science and Engineering
 University of California, San Diego
 San Diego, 9500 Gilman Drive, La Jolla, CA 92093, USA

Z. Nie, Dr. S. Yang, Prof. X. Zhang
 Department of Mechanical Engineering
 University of California, Berkeley
 Berkeley, CA 94720, USA

C. Posner, Prof. J. Zhang
 Department of Pharmacology
 University of California, San Diego
 San Diego, 9500 Gilman Drive, La Jolla, CA 92093, USA

 The ORCID identification number(s) for the author(s) of this article can be found under <https://doi.org/10.1002/adma.202006496>.

DOI: 10.1002/adma.202006496

challenges in achieving a high photostability with a sufficient number of emitted photons.

Herein, we demonstrate an unprecedented fluorophore photostability enabled by a self-assembled organic hyperbolic material (OHM) film^[28] in the visible spectrum. Compared to traditional HMMs^[22,29,30] made of noble metal structures and other natural hyperbolic materials,^[31–33] the OHMs used in this work feature a Lorentz-type dispersion^[33,34] with low-loss natural hyperbolic polariton modes,^[28] and thus support an extremely large LDOS and a large Purcell factor.^[35] Moreover, this low-loss hyperbolic nature of the OHM films also makes an efficient fluorescence enhancement without any outcoupling structure possible. Therefore, it was observed that fluorophores near the OHMs showed a 230-fold increase in the total number of emitted photons, and a 500-fold prolonged photobleaching lifetime simultaneously. Such a remarkably enhanced fluorophore photostability may lead to various new opportunities where photobleaching is a concern.

An OHM of regioregular poly(3-hexylthiophene-2,5-diyl) (rr-P3HT) was self-assembled as described in ref. [28]. Figure S1a in the Supporting Information shows the complex permittivity of the fabricated rr-P3HT OHM film measured by variable angle spectroscopic ellipsometry (VASE). The film features low-loss hyperbolic behavior in the visible spectral range of 420–560 nm with the material figure of merit (FoM) $-\text{Re}(\epsilon_H)/\text{Im}(\epsilon_H) > 10$, where ϵ_H is the horizontal component of the complex permittivity^[28] (see Section S2, Supporting Information). With such a large FoM, the hyperbolic polariton modes supported by the OHM give rise to an exceptionally strong Purcell effect, originating from the excitations of the nonradiative high momentum (high- k) hyperbolic polariton modes (see Section S3, Supporting Information) and the radiative modes (see Sections S4 and S5, Supporting Information). The low-loss hyperbolic nature of the OHMs also leads to a significant increase in the total emitted photon counts through the radiative leaky channel (see Section S5, Supporting Information).

Figure 1a,b illustrates the basic underlying principle of the enhanced photostability of fluorophores by the hyperbolic modes of the OHM. A strong Purcell effect leads to an enhanced spontaneous emission decay rate ($\text{PF} = k_f/k_{f0}$, where k_f (k_{f0}) is a spontaneous emission decay rate of fluorophores on top of the OHM (glass)),^[20–22] which subsequently reduces the probability of photochemical reactions of the fluorophores in the excited triplet state (T_1)^[10–13] (see Section S6, Supporting Information). Note that the Purcell factor (PF) is the sum of the radiative and nonradiative decay rate enhancements, i.e., $k_f/k_{f0} = k_r/k_{r0} + k_{nr}/k_{nr0}$. The presence of the OHM also results in an electric field enhancement ($\Gamma_{\text{exc}} = I_{\text{exc}}/I_0$, where I_{exc} is an electric field intensity in the presence of the OHM). Therefore, the total photobleaching rate $k_{\text{pb,OHM}}$ of fluorophores on top of the OHM can be described by $k_{\text{pb,0}} \times \Gamma_{\text{exc}}/\text{PF}$.^[11,27,36] Note that the subscript 0 represents the corresponding quantities for fluorophores on glass substrate. Since Γ_{exc} with a plane wave is typically ≈ 2 (see Section S7, Supporting Information) while PF is on the order of a few hundreds to a few thousands (Figure 1c), the $k_{\text{pb,OHM}}$ of fluorophores is predominantly determined by the PF provided by the OHM. The enhancement of the total emitted photons (Figure 1d) is $S_{\text{OHM}}/S_0 = \text{PF} \times k_f/k_{f0} = k_r/k_{r0}$,^[11] where S_{OHM} is the total emitted photons in the presence of the OHM. As can be clearly seen from Figure 1c,d, both the PF and S_{OHM}/S_0 are high, so that a strongly suppressed photobleaching of fluorophore (i.e., prolonged photobleaching lifetimes and increase in the total number of emitted photons) is expected with the OHM. Note that the PF can also be large when the fluorophore is placed close to a planar metallic surface, e.g., the PF with a Ag film is about 10^2 at the wavelength $\lambda = 500$ nm. However, the corresponding radiative decay rate enhancement k_r/k_{r0} is only around 1.5 (see Section S4, Supporting Information). Therefore, most of the emitted photons are converted to the nonradiative modes and then dissipated in the metallic film. In contrast, in the case using the OHM, due to the excitation of the low-loss hyperbolic modes and the radiative coupling to

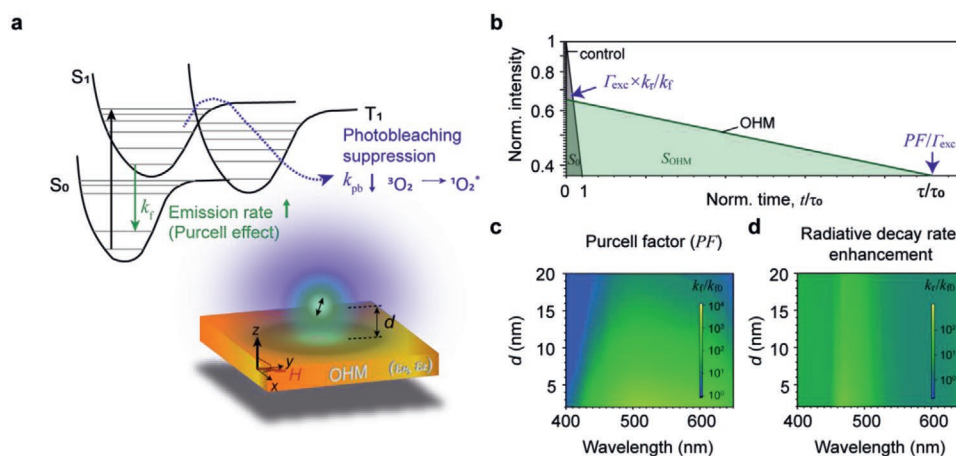


Figure 1. Photobleaching suppression near OHMs. a) Simplified schematic energy diagram and photostability enhancement by the Purcell effect. The Purcell factor (PF) is a key quantity that describes the coupling rate between a dipole emitter and hyperbolic modes of a planar OHM (see the inset). Photobleaching rate k_{pb} of a fluorophore on top of the OHM is inversely proportional to the PF. b) Schematic drawing of the fluorescence intensity over time for fluorophores on glass and on OHM. c) Wavelength and distance dependences of the PF and d) the radiative decay rate enhancement. The PF comes from both the radiative k_r/k_{r0} and the nonradiative k_{nr}/k_{nr0} components. The radiative decay rate enhancement represents the increase of the total number of emitted photons.

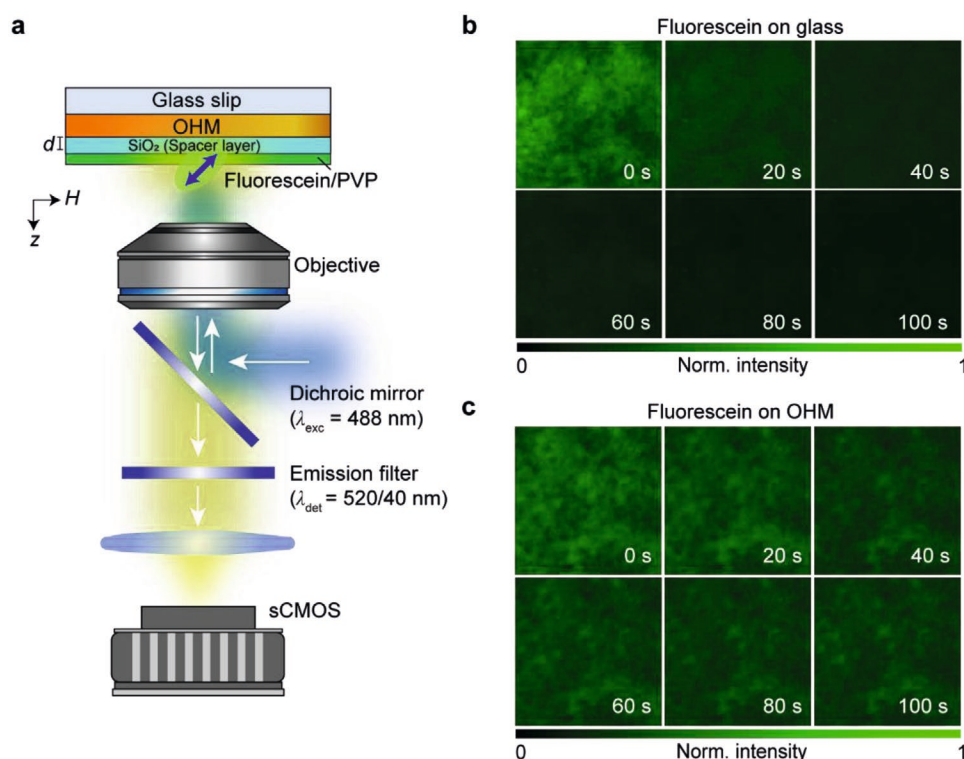


Figure 2. Experimental set-up and photobleaching response of fluorophores on various substrates. a) Experimental set-up. The normalized emission intensity of fluorophores was monitored over time (at 0, 20, 40, 60, 80, and 100 s during the continuous excitation laser exposure on the fluorophore layer). b,c) The emission intensity of fluorescein on a glass coverslip (control sample) (b) and on the OHM film (c).

the far field, there is a significant enhancement in the radiative component, i.e., k_r/k_{f0} reaches to 10^2 ; moreover, a higher k_r/k_{f0} is possible by considering roughened OHM films (see Sections S4 and S5, Supporting Information).

The photobleaching response of a fluorescent molecule refers to a degradation of the photon emission intensity over time; a photobleaching lifetime can be extracted from this response by mathematical fitting. Photobleaching experiments were carried out with a wide-field fluorescence microscope as shown in Figure 2a (see details in the Experimental Section). A 488 nm laser was used to excite molecules of fluorescein (Figure S1b, Supporting Information) situated on top of the OHM films with an intensity of $\approx 61 \text{ W cm}^{-2}$. Note that a nearly constant laser intensity was applied for all experiments to exclude any possible excitation-power dependence on the photobleaching dynamics. To study distance-dependent photobleaching dynamics caused by the distance-dependent PF, SiO_2 spacer layers with respective thicknesses $d = 0, 5, 10$, and 20 nm were sputtered onto four identical OHM films. A fluorescein/poly(vinylpyrrolidone) (PVP) layer with $2\text{--}5 \text{ nm}$ thickness was spin-coated (see details in the Experimental Section) onto the top of the spacer layer. A band-pass filter ($\lambda_{\text{em}} = 520/40 \text{ nm}$) was used to collect emission signals from the fluorescein molecules. 5000 frames of fluorescence images were collected with an exposure time of 200 ms at the imaging speed of $5 \text{ frames per second}$ in order to obtain a complete photobleaching decay curve. To demonstrate enhanced photostability of fluorescein by the OHM in an intuitive way, the wide-field fluorescence images at various times throughout the exposure are shown in Figure 2b,c: On

the glass substrates (Figure 2b), the fluorescein was completely destroyed after $\approx 20 \text{ s}$; however, the emission degradation of the fluorescein on the OHM substrate occurred much more slowly (Figure 2c) and fluorescence was still visible after $\approx 100 \text{ s}$.

A value for photobleaching lifetime can be extracted by fitting the photobleaching decay curve on a pixel by pixel basis. For the photobleaching curve of fluorescein on the control sample, a single-exponential-decay function was used to obtain the photobleaching lifetime τ_0 . For the OHM sample, a bi-exponential decay fitting was applied to the data, showing two photobleaching lifetimes: the first being relatively fast τ_1 , and a second slower τ_2 . This bi-exponential decay response can be interpreted as differences in the PFs arising from surface roughness of the OHM film and nonuniformity in dye layer thickness^[37] (the dye layer contains both strongly and weakly interacting dye molecules on the OHM film). The quick photobleaching τ_1 is attributed to weakly interacting dye molecules located above the coupling distance from the OHM (see details in Section S8, Supporting Information).

The calculated distance-dependent PFs for the experimentally realized distances are given in Figure 3a and the calculated PFs at $\lambda = 520 \text{ nm}$ as a function of the distance to OHM surface are shown in Figure 3b. Figure 3c–f gives the statistics of the photobleaching, obtained from the extracted photobleaching decay time from a $50 \times 50 \text{ pixel}$ ($8.125 \times 8.125 \mu\text{m}^2$) area, showing a lengthening of photobleaching lifetime for fluorescein on an OHM substrate compared to that on a glass substrate. In Figure 3c, most of the dataset show a $200\text{--}1000\times$ improvement, and some of the suppression factors reach a factor of $10\,000\times$.

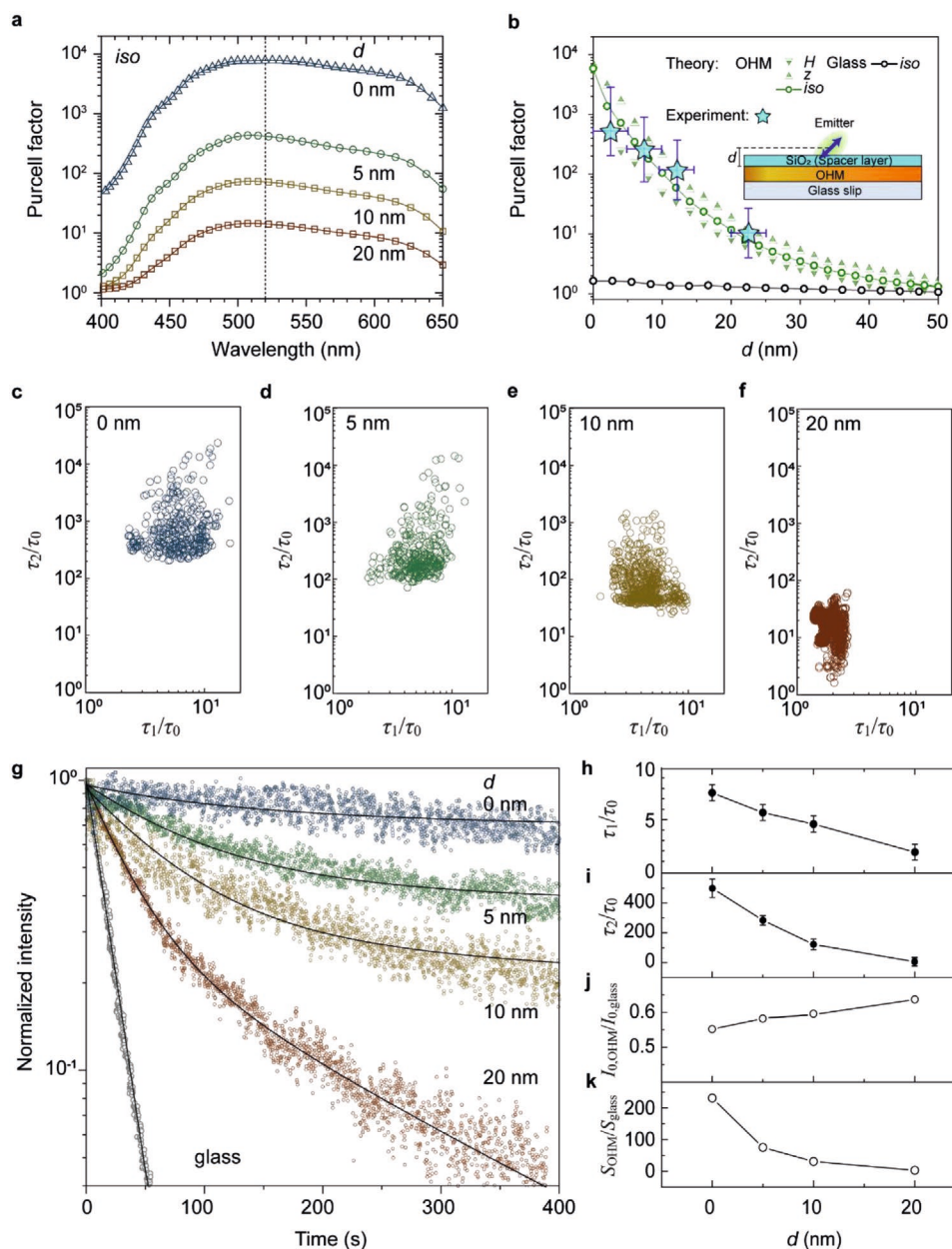


Figure 3. PF and enhanced photostability for fluorescein on an OHM. a) Calculated PF spectra for an isotropic dipole source located at a height of d above the OHM substrate. b) Experimental and calculated PF for dipole sources (dipole direction: parallel is given as H , perpendicular is given as Z , and averaged is given as iso with respect to substrates) located above the OHM (blue curve) and the glass (black curve) substrates at wavelength $\lambda = 520$ nm. c–f) Experimentally measured photobleaching suppression rates (τ_1/τ_0 and τ_2/τ_0) of fluorophores located above the OHM surface for: c) $d = 0$ nm, d) $d = 5$ nm, e) $d = 10$ nm, and f) $d = 20$ nm, respectively. g) Normalized emission intensities as a function of detection time, generated from a 50×50 pixel average corresponding to an area of $8.125 \times 8.125 \mu\text{m}^2$. h) Distance dependence of τ_1/τ_0 . i) Distance dependence of τ_2/τ_0 , where τ_0 corresponds to the photobleaching lifetime of fluorophores on glass. j) Distance dependence of the initial emission intensity $I_{0,\text{OHM}}/I_{0,\text{glass}}$ at $t = 0$, where $I_{0,\text{glass}}$ corresponds to initial emission intensity measured on glass. k) Distance dependence of the integrated emission intensity $S_{\text{OHM}}/S_{\text{glass}} = \sum I_{t,\text{OHM}}/I_{t,\text{glass}}$, where S_{glass} corresponds to integrated emission intensity measured on glass.

Table 1 summarizes these average values, and averaged emission intensity decay curves are given in Figure 3g. A significant modification of the fluorescein photobleaching dynamics resulting from the OHM is apparent. Strong dependence of photostability on distance from the OHM surface was observed; distance-dependent average photobleaching lifetimes are shown in Figure 3h,i. Experimental results are in good agreement with

the calculated PFs (see Figure 3b and Sections S6.2, Supporting Information).

Since the SNR is crucial for fluorescence microscopy, emission intensity I_t per frame and the total emission intensity $S = \sum I_t$ were investigated. In the beginning stage, fluorophores on glass substrate emit more photons than those on the OHM. For example, Figure 3j shows the normalized initial

Table 1. Comparative photobleaching response of fluorescein dye on glass and OHM substrates.

Samples	d [nm]	Photobleaching lifetime		Photobleaching suppression rate		Initial intensity	Total intensity
Glass		τ_0 [s]		τ_0/τ_0		$I_{0,\text{glass}}/I_{0,\text{glass}}$	$S_{\text{glass}}/S_{\text{glass}}$
	0	15.6		1		1	1
OHM		τ_1 [s]	τ_2 [s]	τ_1/τ_0	τ_2/τ_0	$I_{0,\text{OHM}}/I_{0,\text{glass}}$	$S_{\text{OHM}}/S_{\text{glass}}$
	0	119.8	7897.5	7.7	506.3	0.552	231.3
	5	90.1	4547.5	5.8	291.5	0.582	75.3
	10	72.6	2005.6	4.7	128.6	0.596	30.7
	20	31.3	181.7	2.0	11.6	0.637	2.92

emission intensity $I_{0,\text{OHM}}/I_{0,\text{glass}}$ as a function of the distance between fluorophores and the OHM surface; these values are 0.55, 0.58, 0.60, and 0.64 for 0, 5, 10, and, 20 nm separations, respectively. This distance-dependent change in the normalized emission intensity is attributed to the introduction of a nonradiative decay channel due to the OHM loss—in other words, a fraction of emitted photons will be absorbed by the OHM (see details in Section S7, Supporting Information). Nevertheless, as demonstrated above, the photobleaching of fluorophores is much faster on glass than on the OHM (Figure 3g). As a result, above a certain time threshold, more photons are obtained from the OHM sample than the glass sample. Figure 3k shows the normalized total emission intensity $S_{\text{OHM}}/S_{\text{glass}}$ from fluorophores at different distances above the OHM surface; these values are 231, 75, 31, and 3 over the distance of 0, 5, 10, and 20 nm, respectively. This emission enhancement is attributed to the improvement of fluorescence photostability with the OHM since an increased emission time leads to more emitted photons and will give rise to a large SNR.

Fluorescence photostability improvements by the OHM were also clearly observed in bioimaging of a Lifeact-Venus-tagged Cos-7 cell (Figure 4). In these cell images (Figure 4a–d), the emission lifespan on the OHM surface exhibits a stronger photobleaching suppression compared to that of the control sample. Note that the distance of the Cos-7 cells with fluorescently labeled actin and plasma membrane from the substrate varies from 2 to 80 nm.^[27,38] We believe that prolonged photobleaching lifetimes provide long-lasting fluorescence imaging for all fluorophores within the effective range of 0–60 nm (Figure 3b) along the axial direction.

A survey of experimentally obtained PFs in the visible spectrum among the most used HMMs and plasmonic materials, as well as the OHMs is shown in Figure S10 in the Supporting Information. For a given plasmonic material, the Purcell effect originates from the surface plasmon resonance, and the maximum PF is obtained at the resonance peak wavelength. For Ag, the resonance peak wavelength is centered around 440 nm,^[39] and for Au it is centered at 620 nm.^[40–42] TiN-based HMMs,^[43,44] Ag-based HMMs,^[20,21,23,33,45–50] and Au-based HMMs^[40,51,52] support a broadband but relatively small PF. The OHMs used in this work provide PFs two orders of magnitude larger than the values found in those plasmonic materials, and even comparable to the values attained by using plasmonic nanostructures such as nanoantennae,^[11,41] nanocavities,^[53] and nanogratings^[21,48] in the spectral range of 480–560 nm. Note that by exploiting the OHM's dispersion tunability,^[28] the PF and the corresponding operating wavelength can be further optimized.

In conclusion, we demonstrate a novel OHM platform with the record PFs at visible frequencies that significantly enhanced photostability of fluorophores. Fluorophore photobleaching lifetimes were lengthened up to four orders of magnitude with a 230-fold increase in photon counts (see a detailed comparison in Section S12, Supporting Information). The performance can be further improved by, e.g., optimizing the surface roughness and the thickness of OHM films. Such an OHM platform could enable a number of high-performance photonics applications such as organic photovoltaics, dye lasers, and fluorescence-based techniques including single-molecule tracking, biosensing, and various forms of super-resolution fluorescence microscopy. With its chemical tunability, fabrication simplicity,

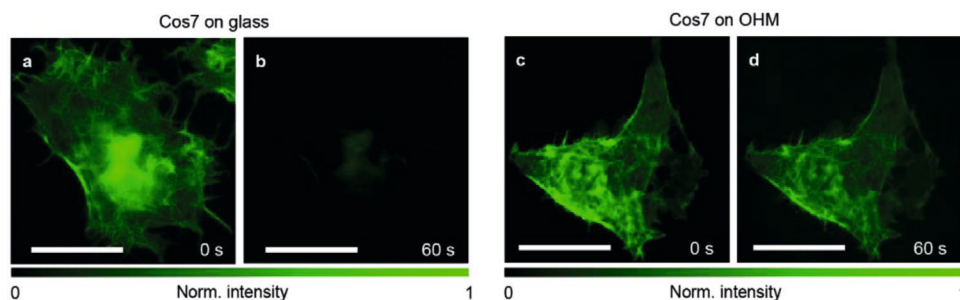


Figure 4. Photostability enhancement. Fluorophores are much more photostable on OHMs than on glass. Lifeact-Venus-tagged Cos-7 cell images are shown after 0 and 60 s of 488 nm excitation laser ($\approx 61 \text{ W cm}^{-2}$) exposure. a,b) On the glass substrate, fluorophores are photobleached almost immediately; c,d) highly photostable fluorophores, however, are observed on the OHM substrate. The scale bars are 20 μm .

mechanical flexibility, and biocompatibility, the demonstrated OHM opens new avenues in nanophotonics.

Experimental Section

Samples for the VASE Measurement: To produce the OHM films, 100 mg of >98% regioregular head-to-tail P3HT molecules (Sigma Aldrich, average $M_w \approx 87\,000\text{ g mol}^{-1}$) was dissolved in 1 mL of chlorobenzene (CB). These solutions were heated to 50 °C for 3 h. The P3HT:CB solutions were spin-coated onto plasma-cleaned glass substrates. Film thicknesses of 182 nm were measured by both a DekTak surface profilometer and VASE. Here, VASE was also used to determine the permittivity spectra of the films. Please see the Supporting Information for details of VASE measurement.

Samples for the Photobleaching Experiment: 1 mg of fluorescein dye was dissolved in 1 mL of combined PVP (Sigma-Aldrich, $M_w = 55\,000$):ethanol solutions (0.01 wt%) to improve fluorophore uniformity in films. The coating solution was dispensed for each OHM film and spun for 5 s at 300 rpm and then 60 s at 5000 rpm. After spin coating, the fluorescein/PVP layer thickness (2–5 nm) was measured with VASE.

Experimental Set-Up: An in-house modified fluorescence microscope (Olympus IX83) was used. Upon excitation with a 488 nm laser (Coherent Genesis MX-488-1000 STM) coupled into a multimode fiber (Thorlabs, core diameter: 50 μm , NA 0.2), the substrate was illuminated with an intensity of $\approx 61\text{ W cm}^{-2}$. Constant laser intensity was applied for all the wide field illuminations in these experiments to exclude the excitation power dependence factor of photobleaching. The fluorescence signal was collected by an objective lens (80 \times /0.6 NA Olympus objective) and sent to an sCMOS camera (Hamamatsu ORCA_Flash4.0 V3 digital CMOS camera (C13440–20CU)) with proper emission filters. A 520/40 nm band-pass filter was used to remove the rr-P3HT emission contribution, and to collect the fluorescein emission. 5000 frames (5 frames per second) of emission signal were acquired and the resulting image stack was analyzed using a mathematical fitting process with in-house developed code run in the MATLAB environment. To synchronize all equipment properly, MATLAB software was run to control a DAQ voltage output module (NI-9263) from National Instruments.

Finite-Difference Time-Domain (FDTD) Calculation: The PF was corresponded to an emission rate enhancement of a spontaneous emitter inside or near a cavity or plasmonic structure. FDTD simulations were performed using the Lumerical software to calculate the dispersion of the PF. By placing a dipole source on top of an OHM/glass substrate at $z = d$, the power emitted from the dipole in the presence of OHM/glass divided by the power emitted from the dipole in the absence of OHM/glass was calculated from 300 to 650 nm. The dipole emitter orientation in the dye layer was assumed to be random. The randomly oriented fluorophore was modeled by an average of 2/3 horizontal (H) dipoles and 1/3 of vertically (z) oriented dipoles. The experimentally obtained permittivity from ellipsometry measurements was used in the FDTD simulations. A minimum mesh step size of 0.25 nm was defined, and the perfectly matched layer's boundary conditions were adopted. The PF calculation included both radiative and nonradiative decay rates associated with near-field coupling to the polaritonic resonance mode of the dipole located nearby the OHM. The dissipated power spectrum was calculated using a band structure simulation methodology. Bloch and PML boundary conditions and time monitors were used to calculate normalized dissipated power spectrum for the randomly oriented and randomly distributed dipoles near the OHM.

Sample Preparation for Lifeact-Venus-Tagged Cos-7 Cells: Cos-7 cells were cultured in Dulbecco modified Eagle medium (DMEM; Gibco) containing 4.5 g L⁻¹ glucose and supplemented with 10% v/v fetal bovine serum (FBS, Sigma) and 1% v/v penicillin-streptomycin (Pen-Strep, Sigma-Aldrich). Cells were maintained in a humidified incubator at 37 °C with a 5% CO₂ atmosphere. 24 h prior to transfection, cells were seeded onto the glass or OHM substrates and grown to 50–70% confluence.

Cells were then transfected with 100 ng of pcDNA3-Lifeact-Venus using Lipofectamine 2000 (Invitrogen) and grown an additional 24 h before imaging.

Supporting Information

Supporting Information is available from the Wiley Online Library or from the author.

Acknowledgements

This work was supported by the Gordon and Betty Moore Foundation. Work at the Molecular Foundry was supported by the Office of Science, Office of Basic Energy Sciences, of the U.S. Department of Energy under Contract no. DE-AC02-05CH11231.

Conflict of Interest

The authors declare no conflict of interest.

Keywords

natural hyperbolic materials, organic hyperbolic materials, photostability, poly(3-hexylthiophenes), Purcell effect

Received: September 23, 2020

Revised: November 30, 2020

Published online: January 27, 2021

- [1] J. W. Lichtman, J.-A. Conchello, *Nat. Methods* **2005**, 2, 910.
- [2] T. Fischer, A. Agarwal, H. Hess, *Nat. Nanotechnol.* **2009**, 4, 162.
- [3] K. E. Preece, E. Drost, N. Hooshyar, A. Krijgsman, P. W. Cox, N. J. Zuidam, *J. Food Eng.* **2015**, 147, 8.
- [4] E. Betzig, G. H. Patterson, R. Sougrat, O. W. Lindwasser, S. Olenych, J. S. Bonifacino, M. W. Davidson, J. Lippincott-Schwartz, H. F. Hess, *Science* **2006**, 313, 1642.
- [5] R. Ameloot, F. Vermoortele, J. Hofkens, F. C. De Schryver, D. E. De Vos, M. B. J. Roelfaers, *Angew. Chem., Int. Ed.* **2013**, 52, 401.
- [6] L. Song, E. J. J. Hennink, I. T. T. Young, H. J. J. Tanke, *Biophys. J.* **1995**, 68, 2588.
- [7] T. Dertinger, R. Colyer, G. Iyer, S. Weiss, J. Enderlein, *Proc. Natl. Acad. Sci. USA* **2009**, 106, 22287.
- [8] L. Shao, P. Kner, E. H. Rego, M. G. L. Gustafsson, *Nat. Methods* **2011**, 8, 1044.
- [9] I. Rasnik, S. A. McKinney, T. Ha, *Nat. Methods* **2006**, 3, 891.
- [10] B. Munkhbat, M. Wersäll, D. G. Baranov, T. J. Antosiewicz, T. Shegai, *Sci. Adv.* **2018**, 4, eaas9552.
- [11] H. Cang, Y. Liu, Y. Wang, X. Yin, X. Zhang, *Nano Lett.* **2013**, 13, 5949.
- [12] I. Kaminska, C. Vietz, Á. Cuartero-González, P. Tinnefeld, A. I. Fernández-Domínguez, G. P. Acuna, *Nanophotonics* **2018**, 7, 643.
- [13] J. V. Pellegrotti, G. P. Acuna, A. Puchkova, P. Holzmeister, A. Gietl, B. Lalkens, F. D. Stefani, P. Tinnefeld, *Nano Lett.* **2014**, 14, 2831.
- [14] A. Poddubny, I. Iorsh, P. Belov, Y. Kivshar, *Nat. Photonics* **2013**, 7, 948.
- [15] L. Ferrari, C. Wu, D. Lepage, X. Zhang, Z. Liu, *Prog. Quantum Electron.* **2015**, 40, 1.
- [16] Z. Liu, H. Lee, Y. Xiong, C. Sun, X. Zhang, *Science* **2007**, 315, 1686.

- [17] J. Sun, M. I. Shalae, N. M. Litchinitser, *Nat. Commun.* **2015**, *6*, 7201.
- [18] N. Vasilantonakis, G. A. Wurtz, V. A. Podolskiy, A. V. Zayats, *Opt. Express* **2015**, *23*, 14329.
- [19] A. D. Neira, N. Olivier, M. E. Nasir, W. Dickson, G. A. Wurtz, A. V. Zayats, *Nat. Commun.* **2015**, *6*, 7757.
- [20] H. N. S. Krishnamoorthy, Z. Jacob, E. Narimanov, I. Kretschmar, V. M. Menon, *Science* **2012**, *336*, 205.
- [21] D. Lu, J. J. Kan, E. E. Fullerton, Z. Liu, *Nat. Nanotechnol.* **2014**, *9*, 48.
- [22] Z. Jacob, I. I. Smolyaninov, E. E. Narimanov, *Appl. Phys. Lett.* **2012**, *100*, 181105.
- [23] Z. Jacob, J.-Y. Kim, G. V. Naik, A. Boltasseva, E. E. Narimanov, V. M. Shalae, *Appl. Phys. B* **2010**, *100*, 215.
- [24] M. A. Noginov, H. Li, Y. A. Barnakov, D. Dryden, G. Nataraj, G. Zhu, C. E. Bonner, M. Mayy, Z. Jacob, E. E. Narimanov, *Opt. Lett.* **2010**, *35*, 1863.
- [25] W. D. Newman, C. L. Cortes, Z. Jacob, *J. Opt. Soc. Am. B* **2013**, *30*, 766.
- [26] A. N. Poddubny, P. A. Belov, P. Ginzburg, A. V. Zayats, Y. S. Kivshar, *Phys. Rev. B* **2012**, *86*, 035148.
- [27] Y. U. Lee, J. Zhao, G. C. H. Mo, S. Li, G. Li, Q. Ma, Q. Yang, R. Lal, J. Zhang, Z. Liu, *Nano Lett.* **2020**, *20*, 6038.
- [28] Y. U. Lee, K. Yim, S. E. Bopp, J. Zhao, Z. Liu, *Adv. Mater.* **2020**, *32*, 2002387.
- [29] S. V. Zhukovsky, O. Kidwai, J. E. Sipe, *Opt. Express* **2013**, *21*, 14982.
- [30] B. Wood, J. B. Pendry, D. P. Tsai, *Phys. Rev. B* **2006**, *74*, 115116.
- [31] E. E. Narimanov, A. V. Kildishev, *Nat. Photonics* **2015**, *9*, 214.
- [32] M. N. Gjerding, M. Pandey, K. S. Thygesen, *Nat. Commun.* **2017**, *8*, 320.
- [33] Y. U. Lee, O. P. M. Gaudin, K. Lee, E. Choi, V. Placide, K. Takaishi, T. Muto, P. André, A. Muranaka, M. Uchiyama, F. Mathevet, T. Aoyama, J. Wu, A. D'Aléo, J.-C. Ribierre, *ACS Photonics* **2019**, *6*, 1681.
- [34] Y. U. Lee, E. Garoni, H. Kita, K. Kamada, B. H. Woo, Y. C. Jun, S. M. Chae, H. J. Kim, K. J. Lee, S. Yoon, E. Choi, F. Mathevet, I. Ozerov, J. C. Ribierre, J. W. Wu, A. D'Aléo, *Adv. Opt. Mater.* **2018**, *6*, 1701400.
- [35] T. Li, J. B. Khurgin, *Optica* **2016**, *3*, 1388.
- [36] K. Vasilev, F. D. Stefani, V. Jacobsen, W. Knoll, M. Kreiter, *J. Chem. Phys.* **2004**, *120*, 6701.
- [37] M. El Kabbash, A. Rahimi Rashed, K. V. Sreekanth, A. De Luca, M. Infusino, G. Strangi, *J. Nanomater.* **2016**, *2016*, 4819040.
- [38] P. Kanchanawong, G. Shtengel, A. M. Pasapera, E. B. Ramko, M. W. Davidson, H. F. Hess, C. M. Waterman, *Nature* **2010**, *468*, 580.
- [39] A. Neogi, C.-W. Lee, H. O. Everitt, T. Kuroda, A. Tackeuchi, E. Yablonovitch, *Phys. Rev. B* **2002**, *66*, 153305.
- [40] N. Tsurumachi, H. Izawa, R. Tomioka, T. Sakata, M. Suzuki, Y. Tanaka, F. Shimokawa, S. Nakanishi, *Jpn. J. Appl. Phys.* **2016**, *55*, 02BB05.
- [41] T. B. Hoang, G. M. Akselrod, C. Argyropoulos, J. Huang, D. R. Smith, M. H. Mikkelsen, *Nat. Commun.* **2015**, *6*, 7788.
- [42] A. I. Chizhik, J. Rother, I. Gregor, A. Janshoff, J. Enderlein, *Nat. Photonics* **2014**, *8*, 124.
- [43] M. Y. Shalaginov, V. V. Vorobyov, J. Liu, M. Ferrera, A. V. Akimov, A. Lagutchev, A. N. Smolyaninov, V. V. Klimov, J. Irudayaraj, A. V. Kildishev, A. Boltasseva, V. M. Shalae, *Laser Photonics Rev.* **2015**, *9*, 120.
- [44] G. V. Naik, B. Saha, J. Liu, S. M. Saber, E. A. Stach, J. M. K. Irudayaraj, T. D. Sands, V. M. Shalae, A. Boltasseva, *Proc. Natl. Acad. Sci. USA* **2014**, *111*, 7546.
- [45] H. I. Lin, K. C. Shen, Y. M. Liao, Y. H. Li, P. Perumal, G. Haider, B. H. Cheng, W. C. Liao, S. Y. Lin, W. J. Lin, T. Y. Lin, Y. F. Chen, *ACS Photonics* **2018**, *5*, 718.
- [46] K. J. Lee, Y. U. Lee, S. J. Kim, P. André, *Adv. Mater. Interfaces* **2018**, *5*, 1701629.
- [47] K. M. Morozov, K. A. Ivanov, D. de Sa Pereira, C. Menelaou, A. P. Monkman, G. Pozina, M. A. Kaliteevski, *Sci. Rep.* **2019**, *9*, 9604.
- [48] D. Lu, H. Qian, K. Wang, H. Shen, F. Wei, Y. Jiang, E. E. Fullerton, P. K. L. Yu, Z. Liu, *Adv. Mater.* **2018**, *30*, 1706411.
- [49] L. Li, W. Wang, T. S. Luk, X. Yang, J. Gao, *ACS Photonics* **2017**, *4*, 501.
- [50] M. Y. Shalaginov, S. Ishii, J. Liu, J. Liu, J. Irudayaraj, A. Lagutchev, A. V. Kildishev, V. M. Shalae, *Appl. Phys. Lett.* **2013**, *102*, 173114.
- [51] K. V. Sreekanth, A. De Luca, G. Strangi, *Sci. Rep.* **2013**, *3*, 3291.
- [52] H.-I. Lin, K. Shen, S. Lin, G. Haider, Y. Li, S. Chang, Y. Chen, *Sci. Rep.* **2018**, *8*, 9469.
- [53] V. J. Sorger, N. Pholchai, E. Cubukcu, R. F. Oulton, P. Kolchin, C. Borschel, M. Gnauck, C. Ronning, X. Zhang, *Nano Lett.* **2011**, *11*, 4907.